Available online at www.sciencedirect.com
ScienceDirect
Carbohydrate Research 343 (2008) 1835–1839
Carbohydrate RESEARCH

Note

A theoretical analysis of the Ti(IV)-catalyzed glycoaminocyanation reaction

Elena Soriano,[a,*] José Marco-Contelles,[b] Hélène Ducatel,[c] Albert Nguyen Van Nhien[c] and Denis Postel[c]

[a]*Laboratorio de Resonancia Magnética, Instituto de Investigaciones Biomédicas (CSIC), C/Arturo Duperier, 4, 28029-Madrid, Spain*
[b]*Laboratorio de Radicales Libres (CSIC), C/Juan de la Cierva, 3, 28006-Madrid, Spain*
[c]*Laboratoire des Glucides, UMR 6219, Université de Picardie-Jules Verne, 33 rue Saint Leu, 80039 Amiens, France*

Received 6 February 2008; received in revised form 5 March 2008; accepted 9 March 2008
Available online 15 March 2008

Abstract—The chelation of the Lewis acid Ti(O*i*Pr)$_4$ provides the necessary conformational control to induce π-facial selectivity on the cyanation process. The steric hindrance imposed by the α-substituent restrains the addition for L-amino acid derivatives.

Keywords: Stereoselective reactions; Titanium; Lewis acid; DFT methodology

Today amino acids are widely used as optically active starting materials for a variety of synthetic applications. Hybrids of sugars and amino acids, also termed as glycosamino acids, are highly polyfunctionalized molecules that combine the structural features of simple amino acids with those of simple carbohydrates. These conformationally restricted building blocks have been used extensively for the preparation of modified analogues of biologically active peptides and/or oligosaccharides.[1]

In a recent communication some of us have described the synthesis of novel glycine-like amino acids from carbohydrate-derived α-aminonitriles as building blocks for peptide synthesis.[2] The aim was the preparation of glycopeptide mimics by introducing an α-amino acid segment onto a saccharide moiety, being the N-terminal group directly linked to a sugar carbon atom (amino sugar–amino acid hybrid **A**, see Scheme 1). The key step in this approach was the Strecker-like reaction of ulose **1** with several protected D- or L-aminoacids leading exclusively, via **2**, to the expected adducts **3** (Scheme 1) with total diastereoselection. After some experimentation, it was observed that Ti(O*i*Pr)$_4$ was a mild and effective Lewis acid[3] for this reaction, but very interestingly, compounds **3** were always obtained in better yields when using D-aminoacid derivatives as precursors.

As shown for D-alanine, compound **3** was obtained in 33% yield, while the yield dropped to 18% when L-alanine was the starting material. These differences in the reactivity of L- versus the D-series could be attributed to an enhancement of the steric constraint on the Ti-complexed transition state induced by the α-substituent.

Prompted by these interesting synthetic results, and in the context of our current work on the DFT-based analysis of reaction mechanisms,[4] we have investigated the stereochemical outcome of this glycoaminocyanation reaction to find an explanation for the observed results, which could be useful for improving and developing more diastereoselective and efficient reactions of this type.

In the presence of the Lewis acid Ti(O*i*Pr)$_4$, chelation between the imine and carbonyl functionalities of the protected aminoacid affords the conformationally fixed chelates $\mathbf{2}_D$ and $\mathbf{2}_L$ (Fig. 1). It is well known that titanium(IV) can accommodate up to six ligands in the coordination sphere.[5] The chelate complexes show a distorted octahedral coordination around the metal, where

* Corresponding author. Tel.: +34 91 585 46 33; fax: +34 91 585 45 87; e-mail: esoriano@iib.uam.es

0008-6215/$ - see front matter © 2008 Elsevier Ltd. All rights reserved.
doi:10.1016/j.carres.2008.03.016

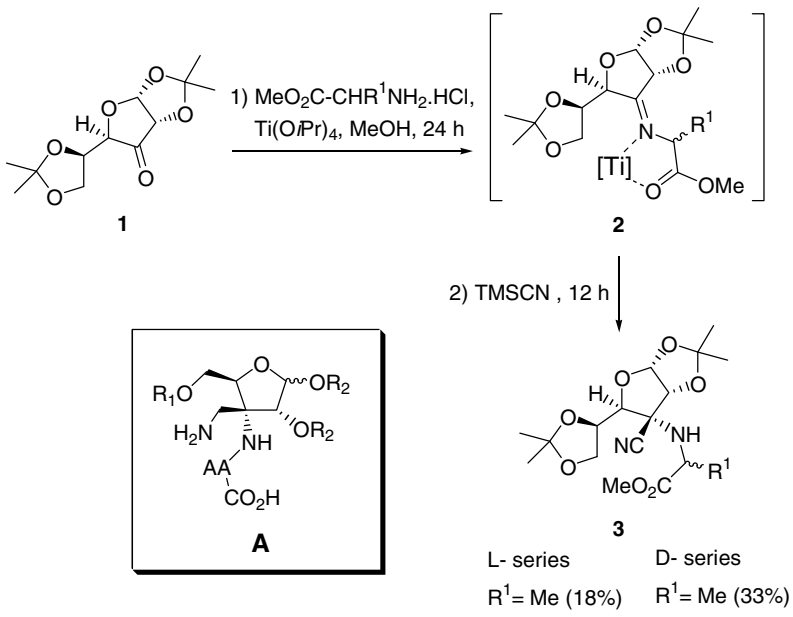

Scheme 1.

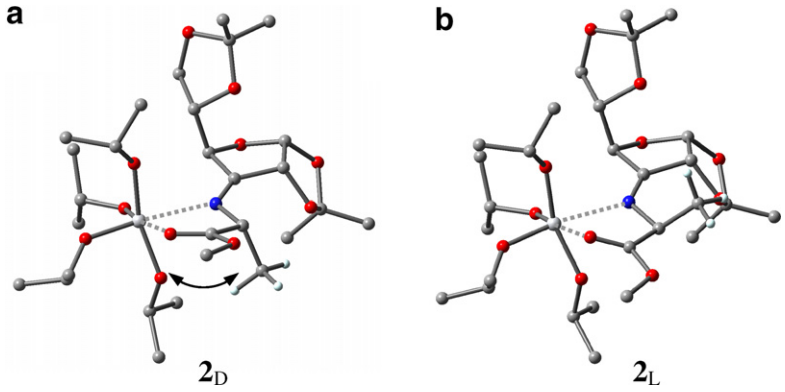

Figure 1. (a) Optimized geometry of $\mathbf{2}_{D}$ showing the unfavorable steric interactions between the alkoxy ligand and the side chain of the protected amino acid, which induce the torsional variation (O1–C2–C3–N4 angle). (b) Optimized geometry of $\mathbf{2}_{L}$. Hydrogen atoms, except at α-methyl group, have been omitted for clarity.

the nitrogen and carbonyl oxygen ligands occupy equatorial positions. Some structural parameters are depicted in Table 1.

It is noteworthy that the Ti–O_1 interaction (carbonyl moiety) appears weaker (longer distance) for the L- than for the D-series (2.331 vs 2.307 Å, in $\mathbf{2}_{L}$ and $\mathbf{2}_{D}$, respectively, Table 1). This is probably due to steric effects arising from the aminoacid side chain. The methyl group for the D-derivatives generates steric repulsions with the axial alkoxy coordinated ligand, which is relieved through a distortion of the dihedral angle O1–C2–C3–N4 (17.4°), as compared with the uncomplexed reactant system (9.3°) and with the L-series (−9.2°), inducing such different Ti–O1 distance (Fig. 1).

In both reactant complexes $\mathbf{2}_{D}$ and $\mathbf{2}_{L}$, the alkoxy ligands and the 1,2-*O*-isopropylidene group in the anomeric position (fused at C-1 and C-2) induce strong steric effects inhibiting a possible nucleophilic attack to the activated C=N bond from the α face of the sugar ring. Therefore, a π-facial selectivity is promoted by chelation, which results in the conformational control over the essential steric interactions and leads to the selective formation of the β-derivative. As can be deduced from Figure 1, the 5-O-protecting group also plays an unfavorable steric role in both the cases for the addition to the β-face, in such a way that a less bulky group should improve the addition yield.

Finally, in the $\mathbf{2}_{L}$ complex the C_{α}-methyl group of the amino acid is oriented toward the β-face, additionally obstructing the nucleophilic attack also from the β-face. This can be easily visualized in Figure 2, where the LUMO orbital, mainly located on the imine moiety, has been mapped onto the electron density surface computed approximately at the van der Waals suface.

Table 1. Structural parameters (in Å and °) of the optimized structures at DFT level

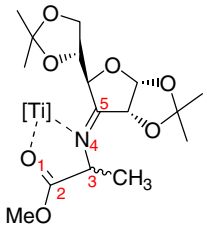

Parameter[a]	$\mathbf{2_D}$	$\mathbf{TS_D}$	$\mathbf{I_D}$	$\mathbf{2_L}$	$\mathbf{TS_L}$	$\mathbf{I_D}$
Ti–O1	2.307	2.321	2.330	2.331	2.300	2.364
Ti–N4	2.379	2.249	2.121	2.363	2.254	2.106
C_{CN}–N_{CN}	1.191	1.182	1.167	1.191	1.184	1.167
C_{CN}–C5	—	2.338	1.482	—	2.307	1.484
N4–C5	1.279	1.307	1.475	1.277	1.305	1.468
O1–C2	**1.241**	1.241	1.244	1.240	1.248	1.244
Ti–O[b]	1.829	1.848	1.844	1.829	1.845	1.844
Ti–O[c]	1.816	1.843	1.885	1.815	1.852	1.878
O1–Ti–N4	70.9	72.6	75.2	70.7	71.2	75.1
Ti–O1–C2	117.1	113.2	110.2	110.0	113.9	109.0
Ti–N4–C3	113.9	116.3	114.6	112.4	109.0	110.5
N_{CN}–C_{CN}–C5	—	153.9	171.7	—	117.9	170.9
C_{CN}–C5–N4	—	99.1	110.5	—	99.7	110.1
O1–C2–C3–N4	17.4	8.3	13.6	−9.2	38.7	31.4

[a] C_{CN} and N_{CN} refer to the attacking cyanide group.
[b] Alkoxy ligand trans to the carbonyl ligand.
[c] Alkoxy ligand trans to the imine ligand.

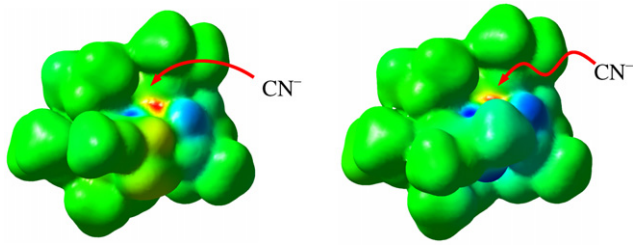

Figure 2. LUMO map computed on the electron density at the van der Waals surface for $\mathbf{2_D}$ (left) and $\mathbf{2_L}$ (right). The nucleophilic attack is more impeded for the L-series.

Consequently, these highly ordered structures $\mathbf{2_D}$ and $\mathbf{2_L}$, with restricted degrees of freedom, will show a somewhat different behavior in a nucleophilic addition step. The cyanide nucleophilic attack takes place through the transitions structures $\mathbf{TS_D}$ and $\mathbf{TS_L}$, respectively, where the CN vector approaches bent to the π face of the acceptor group. As can be deduced from the optimized parameters (Table 1), the most remarkable difference for both the transition structures arises from the C_{CN}–C5 forming bond length. The computed distance for $\mathbf{TS_D}$ (2.338 Å) is longer than that for $\mathbf{TS_L}$ (2.307 Å), suggesting an earlier transition state. Regarding this parameter, the attack of the nucleophile is obstructed for both derivatives due to the bulky groups on the acceptor system (sugar ring and alkoxy ligand). Indeed, our preliminary analysis showed shorter C_{CN}–C5 distances (about 2.24 Å, not shown) for transition structures related to systems less impeded, that is, bearing less bulky substituents on the sugar ring and as coordinating ligands (–OMe). Moreover, the C_α-methyl group of the protected amino acid for the L-derivative induces an additional steric hindrance which cannot be relieved by further structural distortions, due to the highly constrained acceptor structure.

The transition structures $\mathbf{TS_D}$ and $\mathbf{TS_L}$ evolve to the intermediates $\mathbf{I_D}$ and $\mathbf{I_L}$, respectively, which by subsequent N-protonation yield **3**. $\mathbf{I_D}$ and $\mathbf{I_L}$ show the complete formation of the C_{CN}–C5 bond (1.48 Å). As expected, this induces a stronger Ti–N4 interaction which, hence, increases the charge on the metal center and gives rise to a longer Ti–O(alkoxy) distance for the ligand trans to the imino group. Accordingly, the N4–C5 bond length resembles a single methyl-amine bond (1.47 Å). The $sp^2 \rightarrow sp^3$ rehybridization of the acceptor carbon relieves the steric stress and reduces the unstabilizing interaction between the incoming CN moiety and the side chain for the L-series.

The energy values computed must be taken with care because of the solvent model applied. The results showed that nucleophilic addition step takes place with no activation barrier in the gas phase, as other related addition reactions of a charged molecule to a carbon-heteroatom multiple bond have revealed.[6–8] Nevertheless, these processes show activation energy when polar solvent effects are taken into account, due in part to the de-solvation energy associated with the charged molecule. The accurate computational solvent models

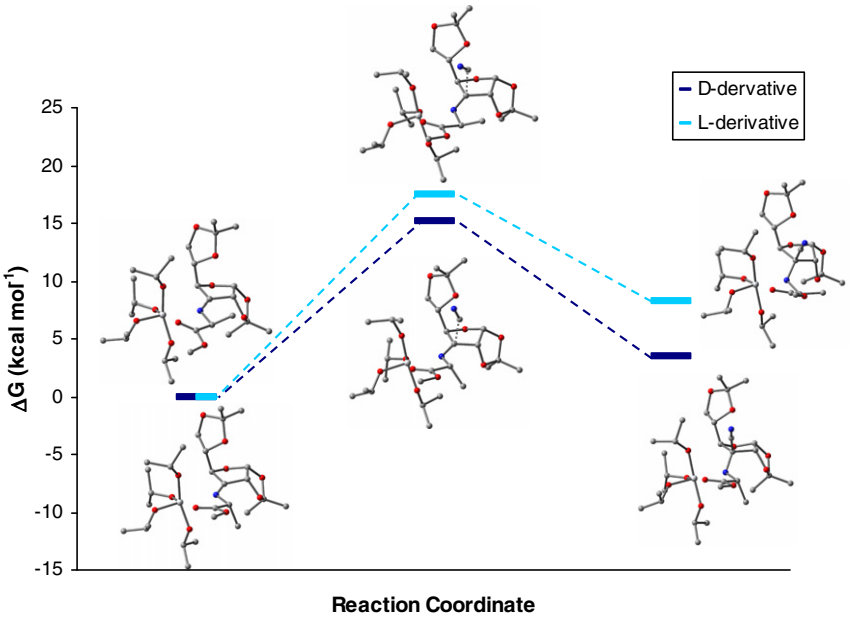

Figure 3. Reaction free-energy profile computed at DFT level.

(PCM) were tested but appeared prohibitive to be applied for the large size structures under study. Therefore, the model applied to take into account the solvent effects was the Onsager model, computationally more accessible but less precise.

The DFT computations reveal that the free-energy barrier for the cyanation step is lower for the D- than for the L-system, 15.12 versus 17.43 kcal mol^{-1}, respectively (Fig. 3). The reaction is slightly endothermic for both D and L series, being $\mathbf{I}_D$ (3.52 kcal mol^{-1}) more stable than $\mathbf{I}_L$ (8.26 kcal mol^{-1}) in relation to reactants. These results suggest that the cyanation is a reversible reaction, where the outcome is governed by kinetic effects. Since electronic properties, such as orbital energy or atomic charge on acceptor atom, appear similar in $\mathbf{2}_D$ and $\mathbf{2}_L$, this difference is mainly due to the steric interactions described above. Therefore, this kinetic preference could account for the experimental results.

To summarize, the chelation of the Lewis acid Ti(O*i*Pr)$_4$ with the carbonyl oxygen atom and imine nitrogen not only improves the efficiency of the nucleophilic addition, but also provides the necessary conformational control to induce π-facial selectivity on the cyanation process for these protected amino acids, and favors the addition for D-series derivatives.

1. Experimental

1.1. Computational methods

Quantum chemical calculations were carried out with the GAUSSIAN 98 (revision A.11) and GAUSSIAN 03 (revision B.03) packages.[9] The starting structures were fully optimized in vacuo with respect to all geometric variables at the B3LYP/3-21G* level of theory, and then single-point energy calculations were performed on the optimized structures with the split-valence B3LYP/6-311+G** basis set to acquire more reliable energy results. Ti atom was described by the quasi-relativistic effective core potential (ECP) by Hay–Wadt.[10] This ECP includes 10 electrons in the core, leaving the outermost 12 electrons to be treated explicitly as valence electrons. Zero-point vibration energy (ZPVE) and thermal corrections (at 298 K, 1 atm) to the energy have been estimated on the basis of the frequency calculations at the optimization level. A comparison of the molecular structures and energetics of a reduced model (–OMe instead of –O*i*Pr as metal ligands, dioxolane instead of dimethyl-dioxolane) using both B3LYP/3-21G* and B3LYP/6-31G* basis sets indicates that an increase in the size of the basis set results in slight changes in the geometrical parameters. While the free-energy differences computed at the B3LYP/6-311+G** are slightly lower for the second set of optimized structures, the relative activation barriers for D versus L series show very similar values. Hence, because full optimization at B3LYP/6-31G* is beyond our computational resources, the adopted approach seems reliable enough to get insights into the selectivity of the process.

The transition structures for the nucleophilic addition were properly characterized by harmonic frequency calculations. The intrinsic reaction coordinate (IRC) pathways from the transition structures were followed using a second-order integration method[11,12] to verify

the expected connections of the first-order saddle points with the appropriate local minima.

Solvent effects were evaluated by the Onsager model.[13,14] The solute radius was computed by a gas-phase molecular volume calculation, and the dielectric constant of the solvent (methanol) applied in our calculations was $\varepsilon = 32.63$.

References

1. Gruner, S. A. V.; Locardi, E.; Lohof, E.; Kessler, H. *Chem. Rev.* **2002**, *102*, 491–514.
2. Ducatel, H.; Van Nhien, A. N.; Postel, D. *Tetrahedron: Asymmetry* **2008**, *19*, 67–81.
3. Reetz, M. T. In *Organometallics in Síntesis*; Schlosser, M., Ed.; J. Wiley & Sons, 1994; pp 195–207.
4. Soriano, E.; Marco-Contelles, J. *J. Org. Chem.* **2007**, *72*, 2651–2654.
5. Pérez, Y.; Morante-Zarcero, S.; Sierra, I.; Gómez-Sal, P.; Fajardo, M.; Otero, A.; Hierro, I. *Inorg. Chim. Acta* **2007**, *360*, 607–618.
6. Pitarch, J.; Ruiz-Lopez, M.; Pascual-Ahuir, J. L.; Silla, E.; Tuñón, I. *J. Phys. Chem. B* **1997**, *101*, 3581–3588.
7. Coll, M.; Frau, J.; Muñoz, F.; Vilanova, B.; Donoso, J.; Blanco, F. G. *J. Phys. Chem B* **2000**, *104*, 11389–11394.
8. Konuklar, F. A.; Aviyente, V.; Ruiz-Lopez, M. *J. Phys. Chem. A* **2002**, *106*, 11205–11214.
9. Frisch, M. J.; Trucks, G. W.; Schlegel, H. B.; Scuseria, G. E.; Robb, M. A.; Cheeseman, J. R.; Montgomery, J.A., Jr.; Vreven, T.; Kudin, K. N.; Burant, J. C.; Millam, J. M.; Iyengar, S. S.; Tomasi, J.; Barone, V.; Mennucci, B.; Cossi, M.; Scalmani, G.; Rega, N.; Petersson, G. A.; Nakatsuji, H.; Hada, M.; Ehara, M.; Toyota, K.; Fukuda, R.; Hasegawa, J.; Ishida, M.; Nakajima, T.; Honda, Y.; Kitao, O.; Nakai, H.; Klene, M.; Li, X.; Knox, J. E.; Hratchian, H. P.; Cross, J. B.; Adamo, C.; Jaramillo, J.; Gomperts, R.; Stratmann, R. E.; Yazyev, O.; Austin, A. J.; Cammi, R.; Pomelli, C.; Ochterski, J. W.; Ayala, P. Y.; Morokuma, K.; Voth, G. A.; Salvador, P.; Dannenberg, J. J.; Zakrzewski, V. G.; Dapprich, S.; Daniels, A. D.; Strain, M. C.; Farkas, O.; Malick, D. K.; Rabuck, A. D.; Raghavachari, K.; Foresman, J. B.; Ortiz, J. V.; Cui, Q.; Baboul, A. G.; Clifford, S.; Cioslowski, J.; Stefanov, B. B.; Liu, G.; Liashenko, A.; Piskorz, P.; Komaromi, I.; Martin, R. L.; Fox, D. J.; Keith, T.; Al-Laham, M. A.; Peng, C. Y.; Nanayakkara, A.; Challacombe, M.; Gill, P. M. W.; Johnson, B.; Chen, W.; Wong, M. W.; Gonzalez, C.; Pople, J. A.; GAUSSIAN 03, Revision B.03, Gaussian, Pittsburgh, PA, 2003.
10. Hay, P. J.; Wadt, W. R. *J. Chem. Phys.* **1985**, *82*, 270–283.
11. Fukui, K. *Acc. Chem. Res.* **1981**, *14*, 363–368.
12. González, C.; Schlegel, H. B. *J. Phys. Chem.* **1990**, *94*, 5523–5527.
13. Wong, M. W.; Frisch, M. J.; Wiberg, K. B. *J. Am. Chem. Soc.* **1991**, *113*, 4776–4782.
14. Wong, M. W.; Wiberg, K. B.; Frisch, M. J. *J. Am. Chem. Soc.* **1992**, *114*, 523–529.